UAlg/TP/98-3
July 1999

# Sphaleron Transition Rate in Presence of Dynamical Fermions

A. Kovner

*Theoretical Physics*
*Oxford University*
*1 Keble Road*
*Oxford OX1 3NP*
*UK*

A. Krasnitz, R. Potting

*Universidade do Algarve*
*UCEH*
*Campus de Gambelas*
*P-8000 Faro*
*Portugal*

We investigate the effect of dynamical fermions on the sphaleron transition rate at finite temperature for the Abelian Higgs model in one spatial dimension. The fermion degrees of freedom are included through bosonization. Using a numerical simulation, we find that massless fermions do not change the rate within the measurement accuracy. Surprisingly, the exponential dependence of the sphaleron energy on the Yukawa coupling is not borne out by the transition rate, which shows a very weak dependence on the fermion mass.

# 1 Introduction.

The 1+1 dimensional Abelian Higgs model merits interest for physical properties it shares with the electroweak theory. In particular, it has topologically distinct minima of the energy, corresponding to different winding numbers of the scalar field. Transitions between these states are possible, at zero temperature through quantum tunneling, and at finite temperature also by thermal activation. What makes these transitions physically very interesting is that they are accompanied by an anomalous change in the fermion number, if the model includes a chiral coupling of the gauge field to fermions. In the electroweak theory, these transitions were, in all probability, responsible for the erasure of the primordial baryon asymmetry. Moreover, they may have led to electroweak baryogenesis. Processes of these type are called sphaleron transitions, owing their name to sphalerons, the lowest-barrier configurations separating energy minima.

Since processes violating the fermion number involve field configurations which are nonperturbatively far from the trivial vacuum, the problem requires a nonperturbative treatment. A useful nonperturbative framework is provided by the Euclidean lattice field theory, wherever processes at zero temperature or static thermal properties are concerned. However, the fermion-number violating processes in question occur in real time and at a finite temperature, and thus are out of reach for the Euclidean quantum theory. The problem simplifies considerably only in the classical approximation. Real-time thermal properties of the resulting classical field theory can be studied numerically after lattice discretization. It has been established recently that, under certain conditions, the classical approximation is reliable for the processes in question [1].

There is by now an extensive body of work devoted to numerical study of the sphaleron transition rate in the classical approximation. Over time, the attention has shifted from one-dimensional models [2, 3, 4, 5, 6] to realistic aproximations of the electroweak theory in 3+1 dimensions [7, 8, 9, 10]. Nevertheless, the one-dimensional models have not yet exhausted their utility. In particular, they can be used to investigate the role of dynamical fermions, such as those present in the standard model, in the real-time processes of interest. While in 3+1 dimensions these degrees of freedom resist classical treatment, such treatment is possible in one-dimensional models upon bosonization. This approach was first proposed by Roberge [12] who used it

to study static properties of sphalerons at a finite fermion density [13]. Here we apply this approach to study the real-time dynamical evolution of the Abelian Higgs model coupled to fermions.

The effect of fermions on sphalerons has been investigated in a variety of ways. These include perturbation theory [17, 18], valence approximation [19], and expansion in the number of fermion families [11]. These methods are used to determine the sphaleron (free) energy rather than the sphaleron transition rate, a dynamical quantity whose determination requires a real-time treatment at finite temperature. Recently Aarts and Smit [20] used the expansion in the large number of families for a numerical study of fermions in a classical Bose field background. The latter method is costly numerically and is yet to yield a figure for the sphaleron rate. To the best of our knowledge, the current work is the first calculation of the sphaleron rate to date to account for dynamical fermions.

The contents of the paper is as follows. In Section 2 we discuss the bosonized form of the model and its vacuum structure. In Section 3 we determine the variation of the sphaleron energy with the Yukawa coupling. Our numerical results for the sphaleron transition rate are presented in Section 4. Section 5 contains the discussion.

# 2 The model

Our starting point is the Lagrangian density in two-dimensional space-time

$$\begin{aligned}\mathcal{L} &= \bar{\psi} i\gamma^\mu(\partial_\mu - ie\gamma^5 A_\mu)\psi - \tfrac{1}{4}F_{\mu\nu}F^{\mu\nu} + \frac{1}{2}(D_\mu\phi)(D^\mu\phi)^* - \frac{\lambda}{4}(|\phi|^2 - v^2)^2 \\ &\quad - y\,[\phi(\bar{\psi}\psi + i\bar{\psi}\gamma_5\psi) + \phi^*(\bar{\psi}\psi - i\bar{\psi}\gamma_5\psi)], \qquad (1)\end{aligned}$$

using the standard notation for the two-component spinor fermions $\psi$, the complex scalar field $\phi$, and the U(1) gauge field $A_\mu$. Here $D_\mu = \partial_\mu - 2ieA_\mu$, where $e$ is the gauge coupling. We assume the fields to satisfy periodic boundary conditions. The scalar self-coupling and the Yukawa coupling are $\lambda$ and $y$, respectively. This model is to be regulated such that the gauged current, $\bar{\psi}\gamma^\mu\gamma^5\psi$ is conserved while the vector current obeys the anomaly equation

$$\partial_\mu\,\bar{\psi}\gamma^\mu\psi \equiv \partial_\mu J^\mu = -\tfrac{e}{2\pi}\epsilon^{\mu\nu}F_{\mu\nu}. \qquad (2)$$

In its global form, the anomaly equation means that the variation of the baryon number $B$ equals that of Chern-Simons number $N_{\rm CS}$:

$$\frac{d}{dt}(B - N_{\rm CS}) = \frac{d}{dt}\left(\int {\rm d}x\psi^\dagger\psi + \frac{e}{\pi}\int {\rm d}x A_1\right) = 0. \tag{3}$$

Better suited for our purposes is the Bose-equivalent form of the Lagrangian:

$$\begin{aligned}\mathcal{L} &= \tfrac{1}{2}\left(\partial_\mu\sigma - \tfrac{e\sqrt{\hbar}}{\sqrt{\pi}}A_\mu\right)^2 - \tfrac{1}{4}F_{\mu\nu}F^{\mu\nu} + \frac{1}{2}(D_\mu\phi)(D^\mu\phi)^* - \frac{\lambda}{4}(|\phi|^2 - v^2)^2 \\ &\quad + Y\left(\phi e^{-2i\sqrt{\pi/\hbar}\sigma} + \phi^* e^{2i\sqrt{\pi/\hbar}\sigma}\right)\end{aligned} \tag{4}$$

This form is obtained by introducing a real scalar field $\sigma$ related to the fermion currents via[1]

$$\begin{aligned}\bar\psi\gamma_\mu\psi &= \frac{\sqrt{\hbar}}{\sqrt{\pi}}\epsilon_{\mu\nu}[\partial_\nu\sigma - \frac{e\sqrt{\hbar}}{\sqrt{\pi}}A_\nu] \\ \bar\psi\gamma_\mu\gamma_5\psi &= \frac{\sqrt{\hbar}}{\sqrt{\pi}}[\partial_\mu\sigma - \frac{e\sqrt{\hbar}}{\sqrt{\pi}}A_\mu]\end{aligned} \tag{5}$$

The vector current obviously obeys the anomaly equation (2).

Two comments are in order with regard to (4). First, note that, in order to satisfy periodic boundary conditions for (4), the field $\sigma$ only needs to be periodic modulo $\sqrt{\hbar\pi}$. Similarly to the winding number of the scalar field, the periodicity mismatch of $\sigma$, $\int {\rm d}x\partial_x\sigma/\sqrt{\hbar\pi}$, changes by an integer under topologically nontrivial gauge transformations. However, unlike the winding number of $\phi$, the periodicity mismatch of $\sigma$ cannot be changed dynamically, because the time derivative of $\sigma$ does satisfy periodic boundary conditions. Thus, imposing periodic boundary conditions on $\sigma$ is a matter of a gauge choice. We will assume $\sigma$ to be periodic in space when we solve the model numerically.

[1]These formulae are slightly different from the standard bosonization formulae which do not contain the vector potential in the bosonized expressions for the currents. The reason for this difference is that in our model the fermions couple to the gauge field through the axial rather than the vector coupling. The Wilson line factor which must be included in the gauge invariant regularized expressions for the fermionic currents are therefore different here from the standard one. The Wilson line in the local limit does not reduce to one and is responsible for the appearance of the vector potential on the right hand side of eq.(5).

Secondly, note that we have included explicitly Planck's constant, obviating the fact that the bosonization essentially links *quantum* theories. In order to determine the loop expansion parameter for the model, we re-express the fields in units of $v$. For convenience, we also express the coordinates in units $1/v\sqrt{\lambda}$. We then obtain for the Lagrangian

$$\begin{aligned}\frac{\mathcal{L}}{\lambda v^4} &= \tfrac{1}{2}\left(\partial_\mu\sigma - g\sqrt{\frac{\hbar}{\pi v^2}}A_\mu\right)^2 - \tfrac{1}{4}F_{\mu\nu}F^{\mu\nu} + (D_\mu\phi)(D^\mu\phi)^* - \frac{1}{4}(|\phi|^2-1)^2 \\ &\quad + \mathcal{Y}\left(\phi e^{-2i\sqrt{\pi v^2/\hbar}\sigma} + \phi^* e^{2i\sqrt{\pi v^2/\hbar}\sigma}\right), \end{aligned} \tag{6}$$

where now $D_\mu = \partial_\mu - 2igA_\mu$, $g = e/\sqrt{\lambda}$ and $\mathcal{Y} = Y/\lambda v^3$. It is now evident that the loop expansion parameter for the model is $\hbar/v^2$. This parameter must be small for the classical approximation to make sense. In the absence of fermions $v^2/\hbar$ is an overall factor in front of the action in path integral. With fermions included, $\hbar/v^2$ appears explicitly in the Lagrangian (6), in such a way that in the range of validity of the classical approximation the gauge coupling of the $\sigma$ field is weak.

The temporal-gauge Hamiltonian density corresponding to (6) is

$$\begin{aligned}\mathcal{H} &= \tfrac{1}{2}\left[E^2 + |P|^2 + \Pi^2 + \left(\partial_x\sigma - \tfrac{g\sqrt{\hbar}}{v\sqrt{\pi}}A\right)^2 + |D_x\phi|^2\right] + \frac{1}{4}(|\phi|^2-1)^2 \\ &\quad + \mathcal{Y}\left(\phi e^{-2iv\sqrt{\pi/\hbar}\sigma} + \phi^* e^{2iv\sqrt{\pi/\hbar}\sigma}\right), \end{aligned} \tag{7}$$

where $A$ is the spatial component of the gauge potential, whereas $E$, $P$ and $\Pi$ are the canonical conjugate momenta of $A$, $\phi$ and $\sigma$, respectively. In the following we solve numerically the equations of motion obtained from this Hamiltonian. It is easy to verify that the time evolution described by $\mathcal{H}$ preserves the local Gauss' constraints

$$\partial_x E - g\sqrt{\frac{\hbar}{\pi v^2}}\Pi - 2ig(P\phi - P^*\phi^*) = 0 \tag{8}$$

While the Hamiltonian (7) is best suited for numerical description of real-time evolution, the static properties of the model are made more transparent by eliminating the $\sigma$ degree of freedom. To this end, we perform the gauge transformation $\sigma \to 0$, $A \to A + v\frac{\sqrt{\pi}}{\sqrt{\hbar}g}\sigma'$ and $\alpha \to \alpha + 2v\sqrt{\frac{\pi}{\hbar}}\sigma$, where $\alpha =$

Arg$\phi$. We also solve the constraint (8) for $\Pi$ and obtain for the remaining degrees of freedom

$$\begin{aligned}\mathcal{H} &= \frac{1}{2}(E^2 + P_\rho^2 + \frac{P_\alpha^2}{\rho^2} + \frac{\pi v^2}{g^2\hbar}(E' - 2gP_\alpha)^2) + \frac{1}{2}\rho^2(\alpha' - 2gA)^2 + \frac{1}{2}\rho'^2 \\ &\quad + \frac{g^2\hbar}{2\pi v^2}A^2 + \frac{1}{4}(\rho^2 - 1)^2 + 2\mathcal{Y}\rho\cos(\alpha), \end{aligned} \tag{9}$$

where $P_\rho$ and $P_\alpha$ are the radial and angular conjugate momenta of the scalar field, respectively. We see that the fermions induce a photon mass $g\sqrt{\hbar/\pi v^2}$. In the classical regime, $\hbar/v^2 \ll 1$, this mass is small compared to $2g$ the photon mass induced by the Higgs mechanism. This form of the Hamiltonian is also used in the following for generating the canonical ensemble of initial configurations at finite temperature.

It is important to understand how the fermions of the original formulation appear in the bosonized version. First, the baryon number in the $\sigma = 0$ gauge is minus the Chern-Simons number:

$$B = -\frac{g}{\pi}\oint dx A\ . \tag{10}$$

Keeping this in mind, we can analyze the vacuum structure of the theory. In the fermion-less Abelian Higgs model, there is an exact degeneracy of vacua labelled by the winding number of the scalar field. In these vacua, related by topologically nontrivial gauge transformations, the Chern-Simons number is equal to the winding number. Not so in the presence of fermions: the minima of the energy correspond to different values of an observable quantity, the fermion number. Hence, these minima are no longer related by a gauge transformation. Moreover, these states have different energies.

To see how this comes about, consider the minimum of the energy (9) for a macroscopically small winding number $n \ll L$, where $L$ is the spatial size of the system. Minimizing the static part of (9) with respect to $A$, we find

$$A = \frac{1}{2g}\frac{1}{1 + \frac{\hbar}{4\pi v^2\rho^2}}\alpha'. \tag{11}$$

In the case $\mathcal{Y} = 0$ we take an ansatz of a constant $\rho$. Using (11), we determine that the constant $\alpha' = \frac{2\pi n}{L}$ minimizes the static energy, and therefore we have the relation

$$n = -[1 + \frac{\hbar}{4\pi v^2\rho^2}]B \tag{12}$$

where $n$ is the winding number of the field $\alpha$. We see that close to the classical limit minima of the energy approximately correspond to integer values of the fermion number. If $\rho$ is constant, so is $\alpha' = 2\pi n/L$, whereas for the constant magnitude of the scalar field one finds $\rho^2 = v^2 + \mathcal{O}((n/L)^2)$. Hence, the scalar self-coupling term in the potential approaches its absolute minimum in the infinite-volume limit. We then obtain for the vacuum energy

$$\mathcal{E}(B)/L = \hbar\pi \frac{B^2}{L^2}(1 + \frac{\hbar}{4\pi v^2}) + \mathcal{O}\left(\frac{B}{L}\right)^4. \tag{13}$$

In the general $\mathcal{Y} \neq 0$ case $\alpha'$ is no longer constant for a minimal-energy winding solution. For simplicity let us consider the limit of the gauge and Yukawa couplings being small compared to the scalar self-coupling: $g \ll 1$, $\mathcal{Y} \ll 1$. Then $\rho$ does not deviate significantly from 1. In the classical limit $\hbar/v^2 \ll 1$ we again have that the baryon number is equal to the winding number of $\alpha$. Consequently one expects that the fermions will appear in the spectrum as the solitons of the field $\alpha$. This indeed is the case. Using (11), we obtain the static equation for $\alpha$:

$$\alpha'' + 2\mathcal{Y}(4\pi \frac{v^2}{\hbar} + 1) \sin\alpha = 0 \tag{14}$$

This is the sine-Gordon equation, which possesses soliton solutions. The mass of the fermion is equal to the energy of the (one-winding) solution[2]

$$M_f = 8\sqrt{\frac{2\mathcal{Y}}{1 + 4\pi v^2/\hbar}}. \tag{15}$$

Similarly, there exist multi-soliton solutions for any $n$. For a vanishingly small fermion density $n/L$ the $n$-fermion state has the energy $nM_f$.

At larger $\mathcal{Y}$ the winding solutions corresponding to fermion excitations look somewhat differently. It is not favourable energetically to keep $\rho$ spatially constant. Instead in the region where the phase $\alpha$ varies between $-\pi$ and $\pi$, the radial field $\rho$ is significantly smaller than its value in the vacuum.

[2]The mass of the fermion in the Lagrangian eq.(4) is given by the relation $M_f = \hbar y v$. This however does not contradict the bosonized result eq.(15) since the relation between the Yukawa coupling $y$ in eq.(1) and the coupling $Y$ in eq.(4) is nonlinear. The standard bosonization procedure leads to $Y \propto y^2$ (taking account of the normal ordering of the exponential of $\sigma$), which is indeed consistent with eq.(15).

This suppresses the contribution of the kinetic energy of the $\alpha$ field to the energy. At very large $\mathcal{Y}$ when the mass of $\alpha$ is larger than the mass of $\rho$ this is obvious since it is the only way to keep down the energetic cost of the winding configuration.

Having discussed the static properties of the model, we can now identify the relevant dimensional scales of the problem. This identification is important for the numerical study presented in the following. Consider the relevant length scales first. These are the fermion (soliton) size of the order $\sqrt{\hbar/(8\pi\mathcal{Y}v^2)}$ and the sphaleron size, of order one (the sphaleron configuration is discussed in some detail in the next section). The system size should be far above, and the spatial discretization (the lattice spacing) far below any of these scales. Next, the relevant time scales are the inverse frequencies $\mathcal{O}(2g)^{-1}$, $\mathcal{O}(1)$, and $\mathcal{O}(2\mathcal{Y}^{-1/2})$ for the gauge, radial scalar, and angular scalar modes, respectively. The time integration step should be chosen well below any of these scales. Finally, consider the relevant energy scales. The sphaleron energy is of order 1. If we wish to be in the range of validity of the sphaleron approximation, we must insist on the inverse temperature $\beta \gg 1$. On the other hand, for the classical approximation to make sense, the temperature must be well above the Higgs ($\mathcal{O}(\hbar/v^2)$), the photon ($\mathcal{O}(2\hbar g/v^2)$), and the $\alpha$-meson ($\mathcal{O}(2\hbar\sqrt{2\mathcal{Y}}/v^2)$) masses. For light fermions, an additional condition relating the temperature and the system size follows from (13). Knowing that the fermion coupling to the gauge field is small in the classical limit $\hbar/v^2 \ll 1$, we can compare this energy to the exact energy for $B$ free massless fermions, $\hbar\pi B(B+1)/L$, whose relative deviation from (13) is $1/B$. The latter is small if a typical value of $B$ is large. At a finite temperature $1/\beta$ this condition is achieved if $\pi\hbar\beta/v^2 \ll L$.

In this work, we use, in view of these considerations, the following choices for the various parameters: gauge coupling $g = \sqrt{2.5}$, Yukawa coupling $0 \leq \mathcal{Y} \leq 0.080$, the loop expansion parameter $\hbar/v^2 = 0.05$, inverse temperature $13 \leq \beta \leq 15$. We performed simulations with the values of $a = 0.25$ and $a = 0.125$ and found no measurable lattice spacing dependence of the transition rate. Similarly, we varied the system length between 250 and 625, and observed no finite size effects.

# 3 The sphaleron

As we know, transitions can occur between the vacua of different winding number. Of interest for the rate of these transitions is the energy of the sphaleron configuration (the lowest energy barrier separating the vacua).

For the massless fermion case ($\mathcal{Y} = 0$), Roberge has shown that the sphaleron configuration is identical to the one in the no-fermion case if the fermion density $n$ is macroscopically small [13].

For the massive case $\mathcal{Y} \neq 0$ the sphaleron solution is not known analytically. Instead, we determined the sphaleron energy, applying the extremization method [14, 15, 16]. The idea is to look for static solutions of the classical equations of motion (including sphaleron configurations) by minimizing the sum of the squares of the right hand sides of the equations of motion for the fields:

$$\mathcal{V} \equiv \sum \left( \frac{\partial V}{\partial \varphi_i} \right)^2 . \tag{16}$$

The sum extends over all the degrees of freedom $\varphi_i$ where $V$ is the potential part of $\mathcal{H}$. The minimization is done using a simple relaxation procedure, *i.e.,* integrating relaxation equations $\partial_\tau \varphi_i = -\partial_{\varphi_i} \mathcal{V}$. In the following, we use the same procedure, with $\mathcal{V}$ replaced by $V$, to measure the integer part of Chern-Simons number.

We used the method as described to determine the height of the sphaleron barrier separating the minima with winding numbers 0 and 1, relative to the absolute minimum of $V$.

The results are displayed in Figure 1.

As is clear from the figure, the sphaleron energy is well approximated by the relation

$$E_{sph}(Y) = E_0 + b\sqrt{\mathcal{Y}} + c\mathcal{Y} \tag{17}$$

where a least squares fit yields $E_0 = 0.942762 \pm 0.000015$, $b = 0.11919 \pm 0.00056$, $c = 3.744 \pm 0.005$. As expected, $E_0$ coincides with the sphaleron energy for massless fermions, which, in turn, is equal to the sphaleron energy in the absence of fermions.

Figure 2 displays the values of the real and imaginary parts of the scalar field ($u$ and $v$) for two configurations, for $\mathcal{Y} = 0$ and $\mathcal{Y} = 0.001$. What is clearly visible is that for $\mathcal{Y} = 0$ the fields passes through zero, and then winds slowly back, through the minimum $u^2 + v^2 = 1$, to the other side of

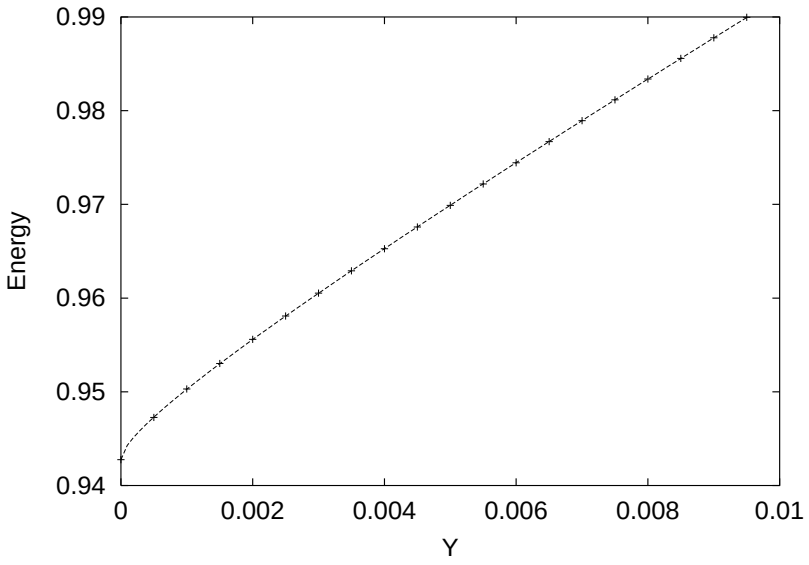


Figure 1: The energy of the sphaleron configuration relative to the vacuum energy. The pluses are the values obtained by the extremization method. The solid curve denotes the least-squares fit to the form $a + b\sqrt{\mathcal{Y}} + c\mathcal{Y}$.

the Mexican hat. For $\mathcal{Y} = 0.001$, the field passes with equal speed over the Mexican hat, but immediately bends toward the minimum at $u = -1$, $v = 0$.

The dependence displayed in (17) can be given a qualitative explanation. The sphaleron energy measures the difference between the energy of the sphaleron configuration and the vacuum energy. The latter corresponds to the absolute minimum of the potential, which occurs, for small positive $\mathcal{Y}$, for a field value close to $-v$. For $\mathcal{Y} = 0$, the sphaleron configuration reduces to the fermionless case

$$\Phi(x) = i \tanh(x/\sqrt{2}) \exp(i\pi x/L). \tag{18}$$

Corrections to the sphaleron energy at a finite $\mathcal{Y}$ can be estimated as follows. First, the phase factor $\exp(i\pi x/L)$ is affected strongly for any finite value of $\mathcal{Y}$. This comes about because, the scalar field must revert to its vacuum value in a finite interval, centered at $x = 0$ to avoid an extensive ($\propto L$) contribution to the sphaleron energy. Much like in the soliton solution of (14), the size of this interval is $\mathcal{O}(\hbar/8\pi\mathcal{Y}v^2)^{1/2}$, in the classical regime

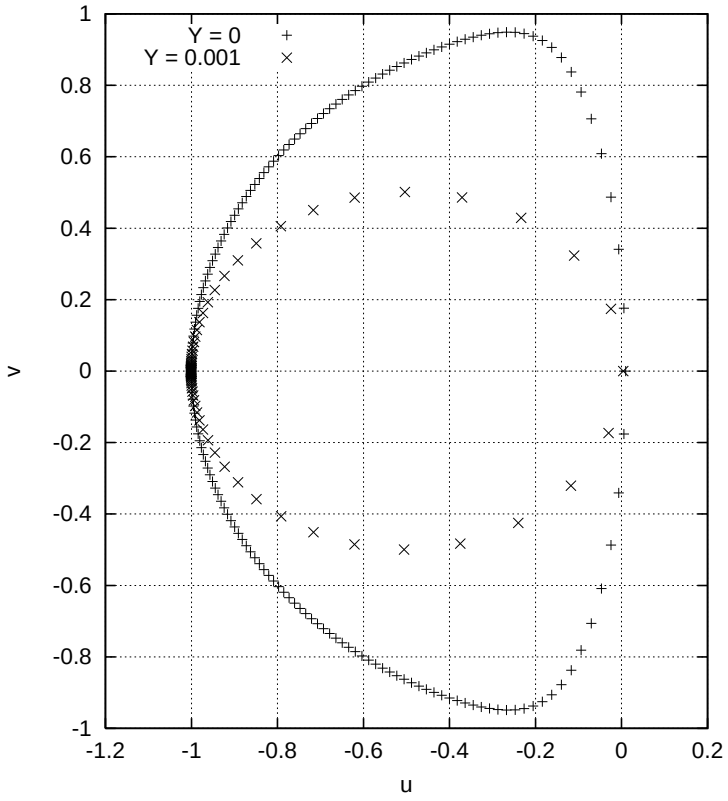


Figure 2: The real and imaginary parts of the scalar field ($u$ and $v$) in the sphaleron configuration, for $\mathcal{Y} = 0$ and for $\mathcal{Y} = 0.001$.

where $\hbar/v^2 \ll 1$. Likewise, the corresponding correction to the sphaleron energy is of the same order as $M_f$ given by (15). As $\mathcal{Y}$ grows and becomes $\mathcal{O}(\hbar/8\pi v^2)$, there occurs a crossover from $\mathcal{O}(\sqrt{\mathcal{Y}})$ to $\mathcal{O}(\mathcal{Y})$ behavior of the sphaleron energy correction, given, in this case, by the spatial integral of the Yukawa term in the sphaleron background.

# 4 The sphaleron transition rate

In the present work, we will be interested in temperatures that are large enough so that quantum effects can be ignored, so that the dynamics is essentially described by classical field theory. Moreover, we will restrict our

attention in this work to temperatures that are small relative to the sphaleron energy, so that the transition rate is suppressed by the factor $e^{-\beta E_{sph}}$. Our choice of the gauge and Yukawa couplings, temperature, linear size, and discretization in space and time is discussed at the end of Section 2.

We use the familiar technique to simulate sphaleron transitions [5]. Namely, we use a combination of Metropolis and heat-bath Monte-Carlo algorithms to draw initial conditions for real-time evolution from the canonical ensemble at temperature $1/\beta$, corresponding to the discretized version of (9). Having generated an initial condition, we switch to the Hamiltonian (7), better suited for real-time evolution. In doing so, we set initially $\sigma = 0$, whereas $\Pi$ is determined by the Gauss' law.

However, the procedure for measuring the sphaleron rate requires modification in the presence of fermions. The rate can no longer be defined, as it was without fermions, as the diffusion constant per unit volume of Chern-Simons number. Indeed, the energy is no longer a periodic function of Chern-Simons number, hence the average squared topological charge can no longer grow linearly with time. We use an alternative measurement method, in which the transitions are counted directly in a real-time simulation. In order to easily identify sphaleron transitions, the field configuration is subjected to relaxation (cooling). A configuration can be thought to represent thermal fluctuations in the vicinity of an energy minimum (a vacuum). The cooling eliminates thermal fluctuations. This is done by solving, for every field $\varphi_i$, the relaxation equation

$$\partial_\tau \varphi_i = -\partial_{\varphi_i} \mathcal{V}. \tag{19}$$

The algorithm is essentially the same as the one employed to determine the sphaleron configurations, but now using the regular static potential $V$ instead of $\mathcal{V}$ given by (16). The resulting cooled configuration has an approximately integer Chern-Simons number, and transitions can be easily counted, as illustrated in Figure 3.

We performed three series of simulations. In the first series we measured the sphaleron transition rate in the Abelian Higgs model without the fermions, where the rate is already known from earlier work [4, 5]. The goal here was to compare the rate obtained by counting transitions to the one found as the diffusion constant of Chern-Simons number. The reliability of the former method depends on the frequency of transitions. If the system size is too large or the temperature is too high, the counting method is not accu-

rate because individual transitions cannot be resolved. We verified that the agreement between the two methods was excellent for all the combinations of sizes and temperatures reported here.

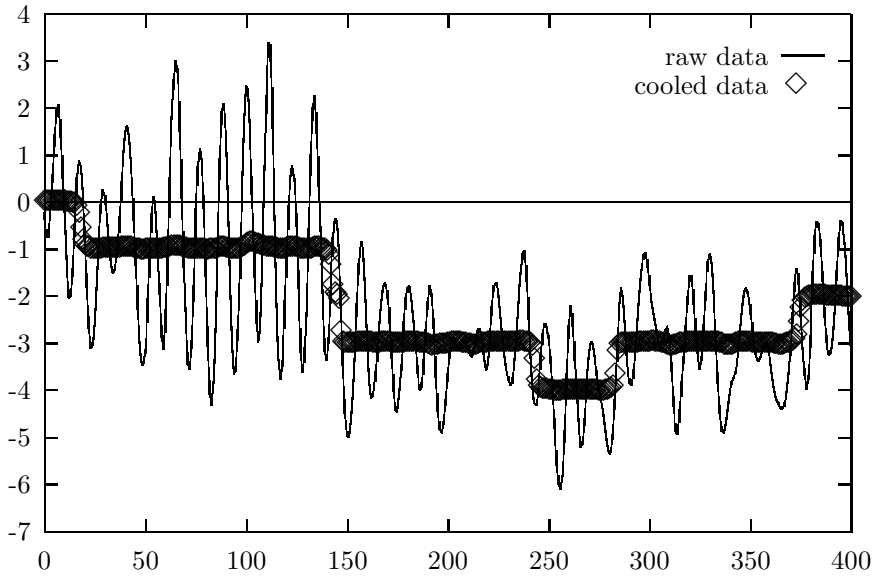


Figure 3: A sample time history of the Chern-Simons number, measured before and after cooling.

In the second series of measurements we determined the transition rate for massless ($\mathcal{Y} = 0$) fermions. Table 1 summarizes the temperature dependence of the rate without and with massless fermions.

| $\beta$ | $\Gamma$ (no fermions) | $\Gamma$ ($\mathcal{Y} = 0$) |
|---|---|---|
| 13 | $(16.2 \pm 0.9) \times 10^{-5}$ | $(16.1 \pm 1) \times 10^{-5}$ |
| 14 | $(7.06 \pm 0.4) \times 10^{-5}$ | $(6.68 \pm 0.34) \times 10^{-5}$ |
| 15 | $(3.06 \pm 0.2) \times 10^{-5}$ | $(3.05 \pm 0.21) \times 10^{-5}$ |

Table 1: A comparative table of transition rate without fermions and with fermions at zero Yukawa coupling.

As is clearly visible, there is no measurable effect of the massless fermions on the rate within the error bars.

In our final series of simulations we investigated the transition rate in the presence of massive fermions. Specifically, the sphaleron transition rate was measured using the cooling/counting method at a fixed values of $\beta$, namely for $\beta = 13$, 14 and 15. We considered values of $\mathcal{Y}$ between 0 and 0.080.

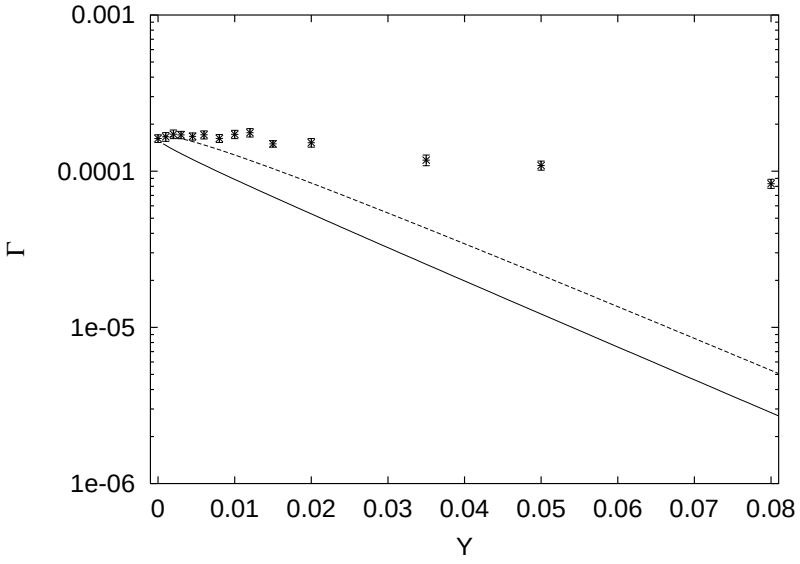


Figure 4: The sphaleron transition rate as a function of Yukawa coupling at $\beta = 13$. The solid curve is $R_u$, the right-hand side of (20). The dashed curve is $R$ as given by (21).

The results are plotted in Figures 4, 5 and 6. As can be seen from the figures, the transition rate, approximately constant as a function of $\mathcal{Y}$ for $\mathcal{Y} < 0.02$, drops off for $\mathcal{Y} > 0.02$, the rate at $\mathcal{Y} = 0.080$ being a factor 2 ($\beta = 13$) to 3 ($\beta = 15$) smaller than at $\mathcal{Y} = 0$. A dropoff of the rate as a function of $\mathcal{Y}$ is exactly what we expect, as the sphaleron energy increases with $\mathcal{Y}$ according to (17). However, this rate dependence on $\mathcal{Y}$ is much weaker than predicted by the sphaleron approximation, which would predict an exponential dropoff (solid line). We discuss this result in more detail in the following section.

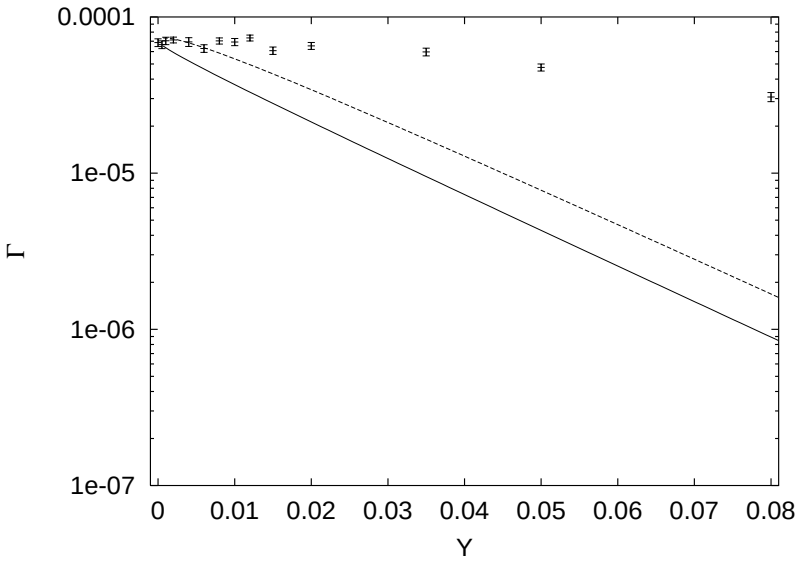


Figure 5: The sphaleron transition rate as a function of Yukawa coupling at $\beta = 14$. The solid curve is $R_u$, the right-hand side of (20). The dashed curve is $R$ as given by (21).

# 5 Discussion

We investigated the effect of dynamical fermions on the sphaleron transition rate, combining bosonization and the classical approximation. As discussed in Section 2, the resulting theory retains important qualitative features expected from the presence of dynamical fermions. This theory is also interesting in its own right, since it helps elucidate the role of additional (other than the gauge field and the Higgs scalar) degrees of freedom in sphaleron transitions. Let us then summarize the lessons learned.

First of all, comparing the rate in the presence of massless fermions to the rate without fermions, we see that, within the error there is essentially effect of including the fermions is a factor that is independent of the temperature for the range of temperatures considered ($12 < \beta < 16$). In other words, the inclusion of fermions does not alter the functional dependence on the temperature. Such behavior agrees very well with what one would expect in the sphaleron approximation for the rate, which, in the absence of fermions,

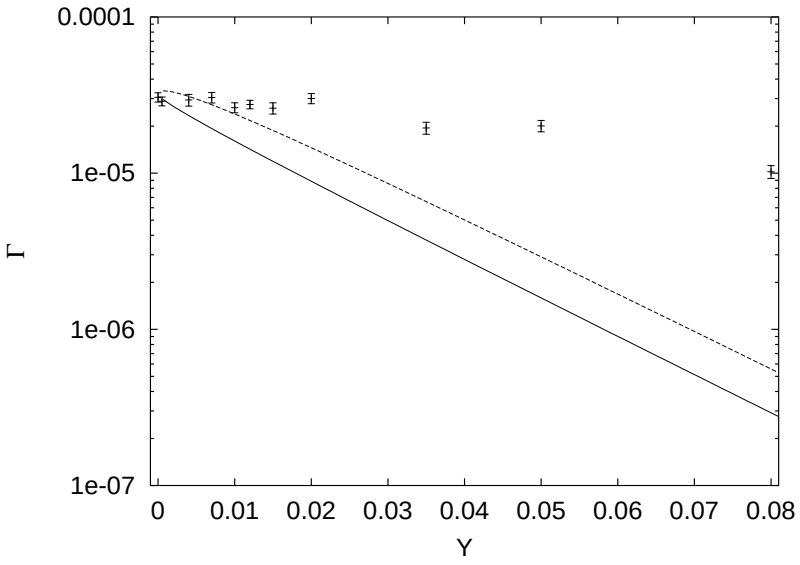


Figure 6: The sphaleron transition rate as a function of Yukawa coupling at $\beta = 15$. The solid curve is $R_u$, the right-hand side of (20). The dashed curve is $R$ as given by (21).

gives

$$\Gamma = \kappa\, T^{2/3} \left(\frac{E_{sph}}{T}\right)^{7/6} e^{-E_{sph}/T}, \tag{20}$$

where $\kappa$ is a numerical constant. In this formula the exponential is the Boltzmann factor of the sphaleron configuration. As we saw in Section 3, massless fermions do not change the sphaleron energy. The temperature dependence of the non-exponential pre-factor results from the existence of zero modes in the sphaleron background which are not present in the background of a vacuum configuration. Massless fermions do give rise to new zero-modes, absent in the no-fermion case. In our model, the new zero-mode is the $\alpha$-meson. However, this mode is not associated with the sphaleron only, it exists both in the sphaleron and the vacuum backgrounds. Hence it cannot change the temperature dependence of the pre-factor.

More interesting is the dependence of the rate on the Yukawa coupling. As one can see from figures 4, 5 and 6, the rate is approximately constant for $0 < \mathcal{Y} < 0.02$, edging down slowly in the range $0.02 < \mathcal{Y} < 0.08$.

We are not aware of, nor do we attempt here, a rigorous determination of the transition rate in the sphaleron approximation in presence of dynamical fermions. However, in a first attempt to understand its dependence on the Yukawa coupling, one might expect that a reasonable first approximation to the rate would be one that based on the rate formula (20) for the fermionless case. The solid curve ($R_u$) in figures 4, 5 and 6 denotes the right-hand side of (20), taking for $E_{sph}$ the $\mathcal{Y}$ dependent value given by (17). It is obvious that the exponential decay as a function of $\mathcal{Y}$ thus predicted is inconsistent with the numerical data.

While we will not resolve this discrepancy in the present work, we would like to point out two possible effects of the fermions on the rate.

The first one is related to the fact that the presence of fermions lifts the degeneracy of the vacuum as a function of Chern-Simons number to the energy of the created (anti)fermion, as is indicated schematically in Figure 5. In the sphaleron approximation the rate is controlled by the sphaleron

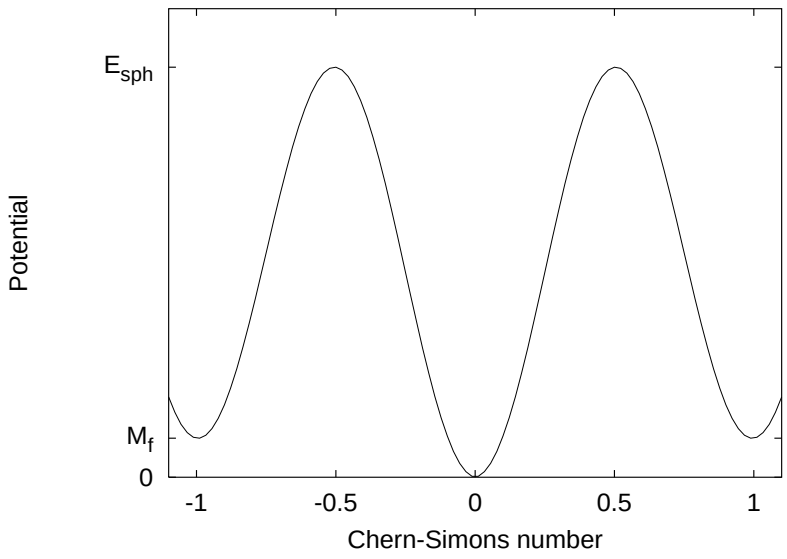


Figure 7: Schematic representation of the effective potential as a function of Chern-Simons number.

energy, or rather, the difference between the sphaleron energy and the vacuum energy. This would be applicable for the rate from the $N_{\rm CS} = 0$ to

the $N_{\rm CS} \approx \pm 1$ state. However, the corresponding Boltzmann factor for the reverse transition is different (larger), due to the energy difference $M_f$ (*cf* (15)), by a factor $e^{\beta M_f}$. The same conclusion is reached by applying detailed balance at temperature $T$.

To compare the sphaleron approximation with the measured rate, we should apply an appropriate averaging over the various types of transitions, that include creation as well as annihilation of (anti)fermions. To this effect, let us consider the following simplified model. Our one-dimensional system can be divided into $g$ intervals of the order of the soliton size. Each interval can be in any of three states: empty, occupied by a soliton (fermion), or occupied by an antisoliton (but not both), each with energy $M_f$. Transitions can take place from the empty state to the soliton or antisoliton state with probability per unit time $R_u$, while the reverse probability is $R_d$, by detailed balance equal to $R_u e^{\beta M_f}$. Direct transitions between soliton and antisoliton state are not possible. The total transition rate will be equal to the $g$ times the (Boltzmann-)averaged transition rate per interval. The latter yields $(2R_u + 2R_d e^{-\beta M_f})/(1+2e^{-\beta M_f}) = 4R_u/(1+2e^{-\beta M_f})$ (the denominator comes from normalization). The total transition rate is simply $g$ times larger. One finds for the total rate

$$R = \frac{4g}{1+2e^{-\beta M_f}} R_u. \tag{21}$$

As $M_f$ is proportional to $\sqrt{Y}$, we thus find a non-trivial $\sqrt{\mathcal{Y}}$-dependent exponential correction. It is to be expected that a similar correction is present in the formula for the effective sphaleron transition rate.

The rate $R$ is plotted for comparison with our numerical data in the Figures 4 through 6. It is obvious that for $\mathcal{Y} > 0.02$ $R$ is still in disagreement with our numerical results. A somewhat better agreement between the data and $R$ at small values of $\mathcal{Y}$ is possibly coincidental, since the description in terms of localized non-overlapping solitons only applies at large $\mathcal{Y}$, such that $\exp(-\beta\mathcal{Y})$ is a small number. We conclude that the near independence of the transition rate on $\mathcal{Y}$ cannot be explained away by the statistical distribution of fermions.

Another possible explanation for the very weak dependence of the rate on $\mathcal{Y}$ is as follows. In the zero fermion mass case one degree of freedom, the phase of the scalar field, is a zero mode, and we have a corresponding Goldstone boson. For $\mathcal{Y} > 0$, the degeneracy is broken, and the Goldstone

boson acquires a mass. However, for very small values of $\mathcal{Y}$, the symmetry remains approximate, and all values of the phase angle remain almost equally occupied. In particular, we can expect a high fermion density. This means that the Gaussian approximation around the field minimum ($\phi \approx -1$) will not be a good one, and one has to apply an appropriate treatment of the Sine-Gordon model instead. We intend to address this point in the future.

# 6 Acknowledgements

A. K. and R. P. wish to acknowledge financial support from the Portuguese Fundação para a Ciência e a Tecnologia, under grants CERN/S/FAE/1177/97 and CERN/P/FIS/1203/98.

# 7 References

1. G. Aarts and J. Smit, Nucl. Phys. B **511**, 451 (1998).
2. D.Yu. Grigorev, V.A. Rubakov, and M.E. Shaposhnikov, Phys. Lett. B **216**, 172 (1989).
3. A.I. Bochkarev and P. de Forcrand, Phys. Rev. D **44**, 519 (1991).
4. A. Krasnitz and R. Potting, Phys. Lett. B **318**, 492 (1993).
5. P. de Forcrand, A. Krasnitz, and R. Potting, Phys. Rev. D **50**, 6054 (1994).
6. W.H. Tang, J. Smit, Nucl. Phys. B **540**, 437 (1999).
7. J. Ambjørn, T. Askgaard, H. Porter, and M.E. Shaposhnikov, Phys. Lett. B **244**, 479 (1990);
   Nucl. Phys. B**353**, 346 (1991).
8. J. Ambjørn and A. Krasnitz, Phys. Lett. B **362**, 97 (1995);
   Nucl. Phys. B**506**, 387 (1997).
9. G.D. Moore, Nucl. Phys. B **480**, 657 (1996);
   Phys. Lett. B **412**, 359 (1997);

Phys. Lett. B **439**, 357 (1998);
Phys. Rev. D **59**, 014503 (1999).

10. G.D. Moore and N. Turok, Phys. Rev. D **56**, 6533 (1997).
11. T. M. Gould and I. Z. Rothstein, Phys. Rev. D **48**, 5917 (1993).
12. A. Roberge, Phys. Rev. D **41**, 2605 (1990).
13. A. Roberge, Phys. Rev. D **49**, R1689 (1994).
14. A. Duncan and R. Mawhinney, Phys. Lett. B **282**, 423 (1992).
15. A. van der Sijs, Phys. Lett. B **294**, 391 (1992).
16. M. G. Perez, P. van Baal, Nucl. Phys. B **429**, 451 (1994); Nucl. Phys. B **468**, 277 (1996).
17. G.D. Moore, Phys. Rev. D **53**, 5906 (1996).
18. D. Diakonov, M. Polyakov, P. Sieber, J. Schaldach and K. Goeke, Phys. Rev. D **49**, 6864 (1994).
19. G. Nolte and J. Kuntz, Phys. Rev. D **48**, 5905 (1993).
20. G. Aarts and J. Smit, "Real-time dynamics with fermions on a lattice", hep-ph/9812413 (1998).
21. A. I. Bochkarev and G. G. Tsitsishvili, Phys. Rev. D **40**, 1378 (1989).